

# Methods to Identify Individual Eddy Structures in Turbulent Flow

Shengwen Wang\*, Jack Goldfeather, Ellen K. Longmire, and Victoria Interrante

**Abstract:** Turbulent flows are intrinsic to many processes in science and engineering, and efforts to elucidate the physics of turbulence are of critical importance to many fields. However, ongoing efforts to achieve a fundamental understanding of the mechanisms of turbulent flow are hindered by the difficulty of quantifying the complex, non-linear interactions between individual eddies in these flows. The difficulty of this task is compounded by the lack of robust methods for accurately identifying individual eddy structures and characterizing their dynamic evolution and organization across multiple scales. In this paper we address this problem by proposing several novel approaches for more accurately segmenting individual eddy structures in turbulent flows.

**Key words:** flow visualization; segmentation; vortices; turbulent flow

## 1 Introduction

Three-dimensional (3-D), time-varying turbulent flows have been a subject of intense research for many years because of their critical importance in many applications. A long-term goal of the ongoing research in the turbulence community has been to develop an improved understanding of the dynamically-evolving eddy structure and organization in various canonical flows, including turbulent boundary layers<sup>[1,2]</sup>. Such improved understanding is critical to the development and validation of accurate numerical models of these flows, which are needed for predictive purposes in engineering and environmental applications. This improved understanding also has the potential to enable the development of effective strategies to control eddy

organization and performance in practical devices.

While many methods have been proposed for defining and visualizing eddies in 3-D flow data<sup>[3]</sup>, little attention has been devoted to the problem of robustly ensuring that the identified regions accurately correspond to individual eddy structures, as opposed to containing entangled clusters of closely spaced and potentially intertwined vortices. However, the success of efforts to effectively analyze the flow dynamics at the level of individual structures critically depends on this ability.

We begin this paper by briefly reviewing current methods for extracting features and defining vortices in 3-D turbulent flows, and explaining their limitations for our purposes. We then outline two novel approaches that we have begun to pursue in our efforts to achieve a robust segmentation of a 3-D flow dataset into individual vortex regions. The first approach is based on the intuition that while any single scalar measure may not provide enough information by itself to robustly define an appropriate segmentation of a composite structure into individual eddies, it is possible that we can do better by considering *multiple*, non-redundant, local scalar, and vector measures in combination. To this end we present a careful mathematical analysis of the interrelationships between swirl and vorticity, and show how these measures can be used together to resolve ambiguities in structure identification that

• Shengwen Wang and Victoria Interrante are with the Department of Computer Science and Engineering, University of Minnesota, Minneapolis, MN 55455, USA. E-mail: wangx549@umn.edu; interran@cs.umn.edu.

• Jack Goldfeather is with the Mathematics and Computer Science Department, Carleton College, Northfield, Minnesota, MN 55057, USA. E-mail: jgoldfea@carleton.edu.

• Ellen K. Longmire is with the Department of Aerospace Engineering and Mechanics, University of Minnesota, Minneapolis, MN 55455, USA. E-mail: ellen@aem.umn.edu.

\* To whom correspondence should be addressed.

Manuscript received: 2013-02-21; accepted: 2013-03-10

cannot be as successfully determined using either measure alone. In a second, different, approach to the problem, we introduce a novel method for automatically detecting potential compound structures in an initial segmentation of a flow and coherently partitioning the constituent components. This method is based on the combined use of vortex core lines and hierarchical region identification. The datasets used in this paper are extracted from a direct numerical simulation of turbulent channel flow in Ref. [4].

## 2 Related Work

Over the years, significant attention has been devoted to the problem of developing robust methods for identifying and effectively visualizing vortical structures in general 3-D flows. Historically, these efforts have been complicated by the lack of a robust, comprehensive, precise mathematical definition of what a vortex is. The most common method of vortex identification is based on the demarcation of regions of swirling flow by threshold levels of a scalar quantity indicative of swirling motion, typically derived from the velocity gradient tensor  $\nabla V$ . Among the suggested criteria are: the  $Q$  criterion<sup>[5]</sup>, the  $\Delta$  criterion<sup>[6]</sup>, the  $\lambda_2$  criterion<sup>[7]</sup>, and swirl strength<sup>[8]</sup>. One complication in using this approach for automatic vortex identification is the need to define an appropriate threshold level to demarcate the region boundary; the spatial extent of the vortex regions identified, as well as the extent to which weak vortices are captured, strongly depends on the threshold level chosen. The use of a scale-space approach, as suggested by Bauer and Peikert<sup>[9]</sup>, offers one possibility to achieve increased robustness; an alternative is to focus on the identification of vortex core lines<sup>[10-14]</sup>. Other promising approaches are the use of a predictor-corrector method<sup>[15-17]</sup> and methods that use Lyapunov exponents to define Lagrangian-coherent structures in time-varying flows<sup>[18-20]</sup>.

## 3 Our First Method

In turbulent flows, the vortices that occur near the boundary often occur in densely intertwined, tightly packed clumps (see Fig. 1, which was obtained from a three-dimensional, high Reynolds number ( $Re = 934$ ), direct numerical simulation of turbulent channel flow<sup>[4]</sup>). In this data, we have found that methods which identify regions of swirling flow, according to any single globally-defined threshold level of a

scalar quantity such as swirl strength, inevitably fail to differentiate individual structures located in close proximity. The three images in Fig. 1 illustrate how reducing the threshold is insufficient to ensure the separation of the individual eddies that otherwise appear connected.

In our first efforts to robustly identify individual vortex structures in turbulent flow, we investigate the extent to which it is possible to achieve a superior segmentation of a flow dataset by using multiple scalar and/or vector flow features in combination rather than relying on a single scalar feature alone. The first step in this process is to identify promising complementary flow features indicative of the presence of a vortex.

We begin by observing that although  $Q$ ,  $\Delta$ , and  $\lambda_2$  represent different scalar measures, the regions

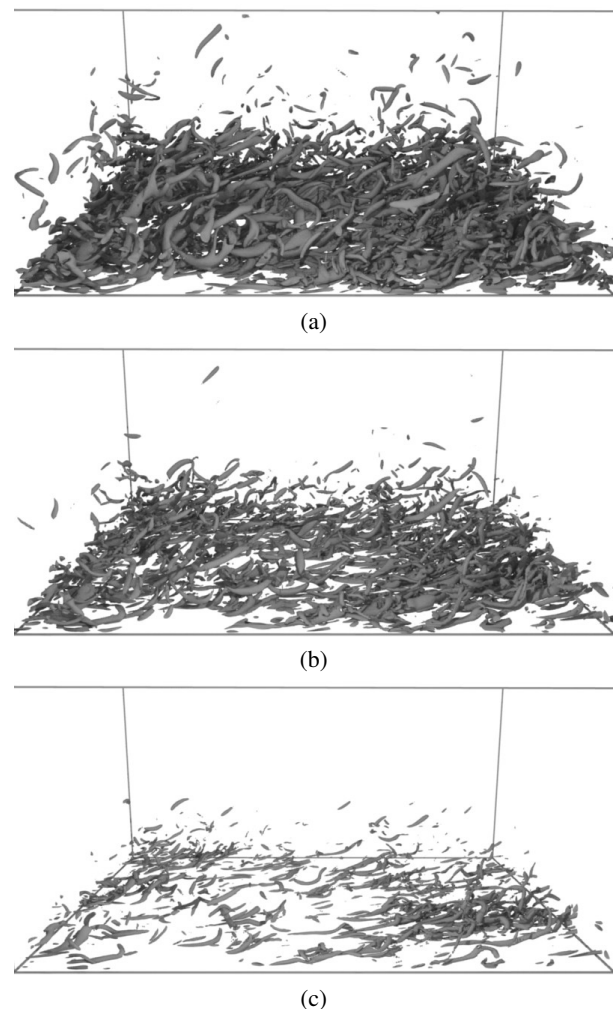


**Fig. 1** Swirling regions are identified at three different threshold levels increasing from top to bottom at 3.5, 5.0, and 8.0. Bottom of plotted domain is the bottom bounding surface. Flow is from left to right.

identified by isosurfaces of each of these quantities are somewhat similar in form in that they are long narrow tubes<sup>[21]</sup>. Hence we investigate the potential of using vector valued features to differentiate neighboring structures.

### 3.1 Definition of vorticity and swirl

There are multiple choices for vectors that describe rotation. For example, the *vorticity* of a velocity vector field  $V$  (also called the *curl* of  $V$ ) is defined as  $\bar{c} = \nabla \times V$ . The direction of this vector  $\bar{c}$  determines the local axis around which rotation occurs as well as the sense of the rotation (using a right-hand rule). The *swirl* of a velocity vector field is defined when two of the eigenvalues of  $\nabla V$  are complex. This measure is designed to differentiate swirling motion about an axis from rotation due to a simple shear, both of which are identified by vorticity. In this case, there is a rotation in the plane determined by the two complex eigenvalues. There are two different ways to think of the axis of this rotation. On the one hand, it is common to think of the normal,  $\bar{n}$ , to this plane as the axis of rotation. On the other hand, the real eigenvector,  $\bar{r}$ , better defines the direction of the swirl isosurface tube (see Fig. 2 and Ref. [8]). We explore using  $\bar{c}$ ,  $\bar{r}$ , and  $\bar{n}$  to segment the vortices.

### 3.2 Relationship between vorticity and swirl

Although  $\bar{c}$ ,  $\bar{n}$ , and  $\bar{r}$  all tell us something about rotation direction in 3-space, in general they each point in a different direction. In order to better understand how vortices change over time and to help us devise disentanglement algorithms, we need to know how these vectors are related mathematically. The following facts can be established (proofs are provided in the appendix).

Let  $\lambda_1 = a + bi$  and  $\lambda_2 = a - bi$  with  $b > 0$  be the complex eigenvalues and  $\bar{v}_1 = \bar{s} + \bar{t}i$  and  $\bar{v}_2 = \bar{s} - \bar{t}i$

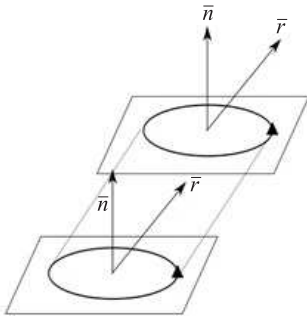


Fig. 2 Swirl rotation axes.

with  $|\bar{s}|^2 + |\bar{t}|^2 = 1$  be the associated eigenvectors of the Jacobian  $\nabla V$  of a velocity vector field  $V$ . Let  $\lambda$  be the real eigenvalue with associated real eigenvector  $\bar{r}$ .

**Theorem 1**  $\bar{c} \circ \bar{n} = b$ , so that the angle  $\theta$  between  $\bar{c}$  and  $\bar{n}$  is given by

$$\cos \theta = \frac{b}{|\bar{c}||\bar{n}|}.$$

An immediate corollary to Theorem 1 is as follows.

**Corollary 1** The swirl  $b$  is always less than half of the magnitude of the vorticity.

Hence regions with high swirl must also have high vorticity.

**Theorem 2** Let

$$B = \begin{pmatrix} \bar{s} \\ \bar{t} \\ \bar{r} \end{pmatrix}, \quad \bar{w} = \begin{pmatrix} (a - \lambda)\bar{s}^T\bar{r} - b\bar{t}^T\bar{r} \\ b\bar{s}^T\bar{r} + (a - \lambda)\bar{t}^T\bar{r} \\ 0 \end{pmatrix},$$

then

$$\bar{r} \times \bar{c} = B^{-1}\bar{w},$$

so that the angle  $\alpha$  between  $\bar{c}$  and  $\bar{r}$  is given by

$$\sin \alpha = \frac{|B^{-1}\bar{w}|}{|\bar{r}||\bar{c}|}.$$

**Theorem 3** If any two of  $\bar{c}$ ,  $\bar{n}$ , and  $\bar{r}$  are in the same direction, so is the third.

These theorems suggest that we may be able to gain insight into how turbulence evolves over time by exploring how the various rotation directions change relative to each other.

### 3.3 Segmenting compound structures using vorticity and swirl

Figure 3 shows a series of images in which structures have been segmented solely on the basis of scalar values of swirl strength. The segmentation is defined as follows. We begin by choosing an arbitrary point whose swirl strength is above the threshold level. We then define the structure to which that point belongs by implementing a recursive flood fill algorithm, adding a neighboring point to the structure if, and only if, its swirl strength is also above the threshold level. When we find that no additional points can be added to a structure, we repeat the process by choosing a new seed point and continue until all points in the volume, whose swirl values are above the threshold, have been tagged as belonging to one structure or another. The structures in each image are each displayed in a different color to clearly label the segmentation. We can see that the lower threshold yields smaller connected regions (e.g., the dark green region in the larger circle in Fig. 3a), but it still remains in a compound form even after the

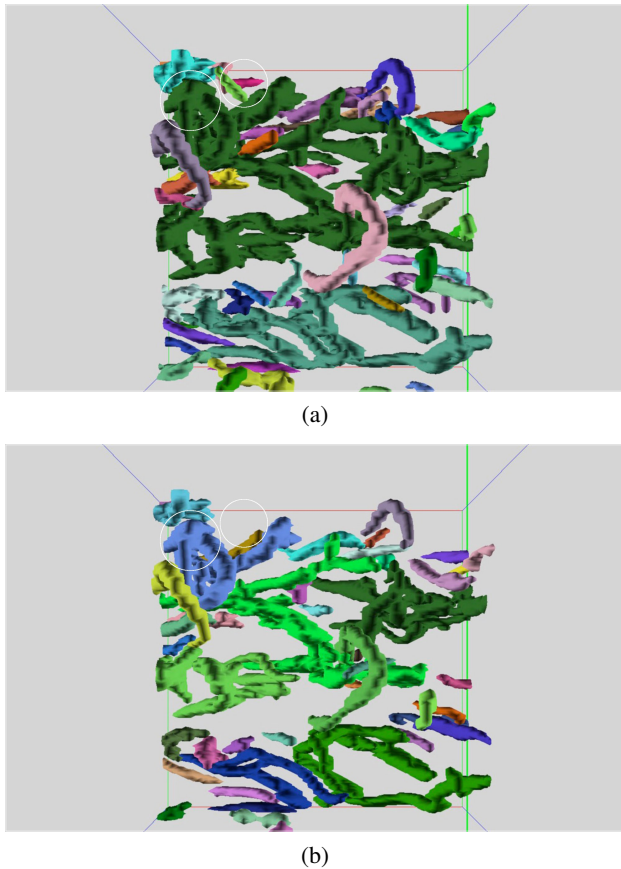


**Fig. 3** Individual vortices segmented according to a threshold level of swirl strength (only), for two different thresholds. Compound form in the bottom image still remains by varying swirl strength only.

threshold has been reduced. It also causes the loss of weaker eddy structures (such as the bright magenta eddy surrounded in the smaller circle).

Figure 4 shows a series of images in which structures have been successfully segmented into proper constituent pieces both on the basis of swirl strength and on the basis of the angles between the directions of  $\vec{c}$ ,  $\vec{n}$ , and  $\vec{r}$  at neighboring voxels. Specifically, the same flood fill approach is used to define a connected region, but in this case a region is expanded to include a neighboring voxel only when the swirl and vorticity directions at that voxel are within a threshold degree of consistency with the swirl and vorticity directions at its neighboring points that have already been identified as belonging to the region. It can be clearly seen that, regardless of the particular threshold values chosen, superior segmentation results are achieved using this combination of scalar and vector flow features than are achieved using swirl strength alone. It can also be seen, by inspection, that introducing the directional

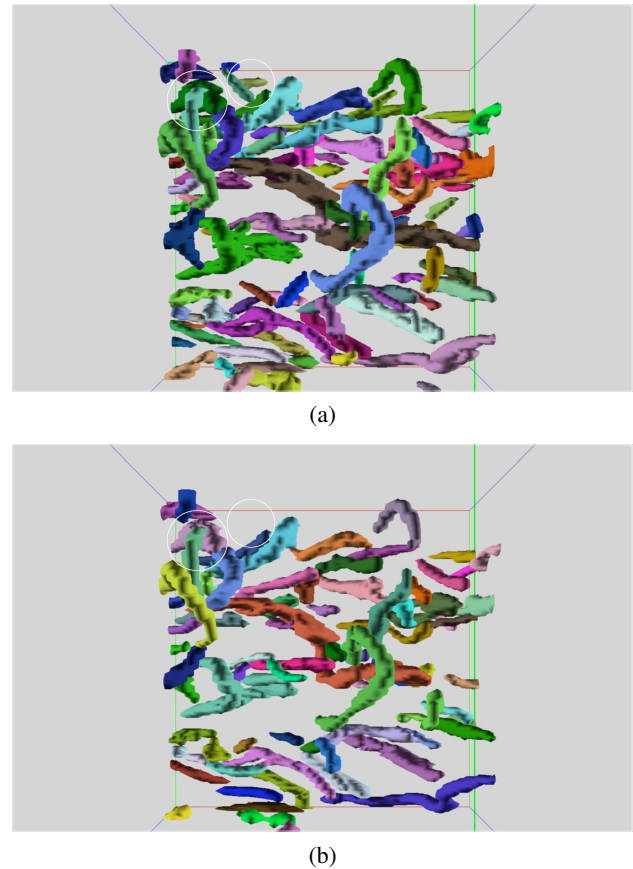


**Fig. 4** Individual vortices defined by similar threshold levels of swirl strength, and by threshold differences between the swirl and vorticity directions at neighboring points. In comparison with Fig. 3, one can see fewer compound structures at each threshold level of swirl strength.

consistency criteria does not result in the spurious subdivision of coherent structures into fragments, even in cases where the vortices are quite bent in their overall shape.

This suggests that there is inherently more promises in an approach that uses both swirl strength and the consistency of swirl and vorticity directions between neighboring points to identify individual vortex structures than in an approach that considers only the level of swirl relative to a threshold. The problem of automatically defining appropriate thresholds of both the scalar quantities and vector differences to use in this process is a separate question, which we intend to address in future work.

### 3.4 Our second method

In this section, we introduce a novel method for automatically identifying individual (potentially compound) structures in a flow, then identifying

individual constituent eddies in each of these structures by leveraging fundamental known characteristics about the physics of flows. Specifically, we make use of the basic intuition that vortices do not branch. Each individual vortex in what appears to be a composite clump will generally be characterized by a separate core line. If we can robustly determine the core line locations, we should be able to use that information to accurately segment each cluster into its true constituent individual eddies as shown in an example of Fig. 5. Essentially, our method works by combining vortex core line detection with hierarchical region identification in Fig. 6.

We begin by identifying a potentially compound structure defined by a connected set of voxels that correspond to locations in the flow where the swirl strength is higher than a specified threshold level. Examples of such structures are shown in red in Fig. 7 above, in the context of other surrounding structures (drawn in grey) within a small region of the flow; the same structure of the image in Fig. 7b is shown in the image in Fig. 8a, in a closer view without the surrounding structures. This initial structure is defined using a simple flood fill algorithm. After the subsequent steps are applied to this structure, another structure is selected, and the process repeats until all voxels in the volume have been classified as belonging to one eddy or another.

Once we have identified a single connected region, shown in Fig. 5a, we begin the process of determining

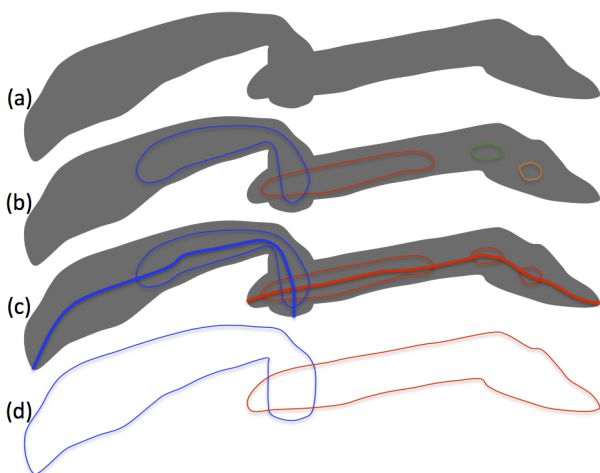


**Fig. 5** An example shows the main steps of our algorithm. (a) The identified primary region as an interesting vortex. (b) The identified subregions as candidate sub-vortices within the primary region. (c) Sub-vortices correlated by extracted vortex cores. (d) Two identified segments shown as blue and red regions.

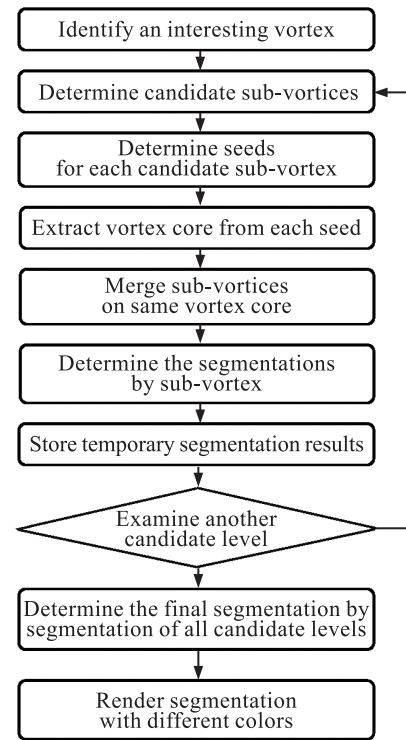


**Fig. 6** A flowchart describing our algorithm.

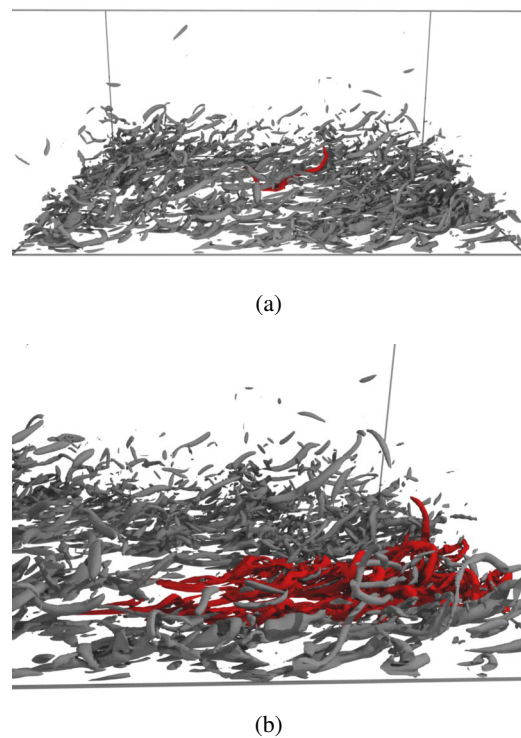


**Fig. 7** Vortices defined by a threshold level of swirl strength. (a) A compound structure that is a region marked in red and is defined by a connected set of neighboring voxels all with supra-threshold values. (b) Another compound structure that is an extremely complex connected region.

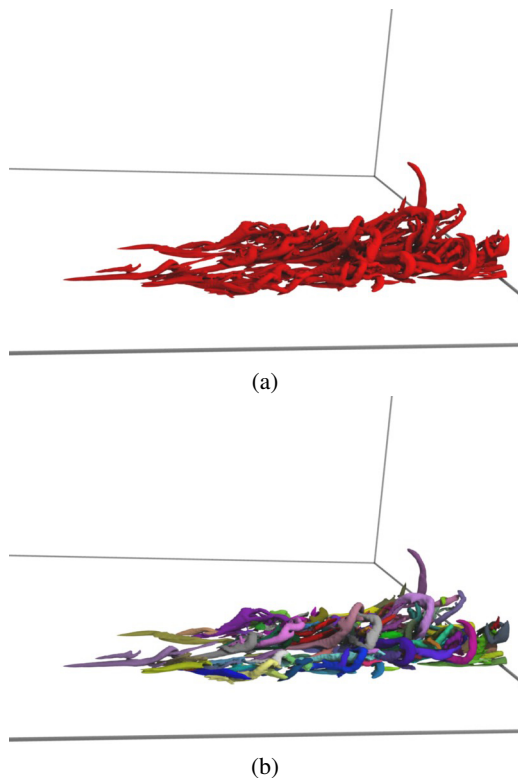


**Fig. 8** (a) A connected collection of voxels delimited by an isosurface of swirl strength. (b) The segmentation of this composite clump into individual eddy structures that is automatically produced by our method.

whether and how it should be subdivided. We start by identifying sub-regions of higher thresholds in the vortex as shown in Fig. 5b. Then, we incorporate the vortex line extraction by identifying a point in a region where the swirl strength assumes a maximal value. We take this point as the seed point from which a vortex core line is grown, in both directions. We define the vortex core line using a variation of the predictor-corrector method described by Banks and Singer<sup>[15]</sup> that relies on vorticity and swirl strength rather than vorticity and pressure for the prediction and correction steps, respectively. This strategy is similar to the approach by Stegmaier et al.<sup>[16]</sup> that replaced pressure of the predictor-corrector method with  $\lambda_2$  for more reliability and applicability. The swirl strength in our line-based method is the quantity that was also used for hierarchical vortex region method. Thus, the identified core line by vortex core detection based on swirl strength benefits the overall procedure of our individual vortex identification.

The criteria we use to determine when to terminate the extension of a vortex core line in the procedure of vortex core detection are as follows. First, we ensure

that the vortex core line does not extend beyond the boundaries of the domain. Second, we stop tracing a core line when the cross sectional area of the portion of the structure through which the core line is currently passing decreases to zero. Third, as a safety precaution, we terminate the growth of a core line if it reaches a total length that is more than twice as long as the longest side of the domain.

After this, we successively consider subregions, within our initial structure, that are defined by decreasing threshold levels of swirl strength, beginning from the maximum value and continuing down to the value that was used to define the extent of the initial structure. At each step in this hierarchical progression, as new subregions develop, we determine whether or not they should be classified as an extension (possibly disconnected) of the existing subregions or as an independent subregion, belonging to a different component vortex in the compound cluster. We make this determination on the basis of the paths taken by the vortex cores through each subregion. If the vortex cores emanating from each region intersect the other region, we consider the two sub-regions as belonging to the same vortex as in Fig. 5c. Because the vortex core line paths can be noisy, we also need to consider additional circumstances. If one of the vortex core lines passes very close to but just misses intersecting the subregion from which the other emanates, and the second subregion is very small, we also consider the two subregions to belong to the same structure. A simple example in Fig. 5 shows steps of one iteration when one threshold value is considered, and two segments are identified in Fig. 5d. We continue this process until all predefined threshold values of swirl strength have been considered.

The groups for each individual vortex core and each of the remaining sub-vortices are all new candidate individual vortex cores. The expansion of the regions from grid cells of individual candidate vortex cores is conducted by a recursive flood fill algorithm that is applied to all sub-vortices simultaneously, and is also similar to the flood approach in our first method. Then, the grid cells within the compound vortex are categorized into different groups, such that each group of grid cells belongs to one of the individual segmented structures.

The previous stage produces a temporary segmentation result for a compound vortex. This result has to be stored so that the program can start over

on another examination with similar processes. We can store these data in memory because the sub-domain we are examining is relatively small and the information we retrieve can be efficiently compacted .

We successively consider subregions, within our initial structure, that are defined by decreasing threshold levels of swirl strength, beginning from the maximum value and continuing down to the one that was used to define the extent of the initial structure. We continue this process until all predefined threshold values of swirl strength have been examined. Our algorithm examines multiple candidate levels, one at a time, to insure that all potential individual vortex cores can be identified. When all levels have been examined, our algorithm proceeds to the next stage.

The final segmentation depends on the segmentations produced at all of the considered threshold levels. Our algorithm examines the results from each iteration and determines the individual vortices across each result. Sub-structures from all candidate levels with the same or closed vortex core lines are considered to belong to the same group. The final segmentation is determined by expanding regions from different final candidate sub-structures. The flowchart in Fig. 6 shows the complete steps of our algorithm.

As a last step, we render each separate group of grid cells using a different color; all primitives are painted according to the color of their group.

Our hierarchical region detection method successfully segments a variety of compound structures into individual vortices, and paints each vortex using a different color. Hierarchical level regions provide premature hints for the candidate segmentation, and the corresponding core lines are used to connect different individual sub-elements together, as shown in Fig. 8. All possible levels are examined to determine the proper categorized regions. Figures 9-11 show more results.

Figure 9 shows a clear success case of our algorithm; a formerly compound structure is successfully segmented into four component pieces. The three images illustrate two intermediate results at different hierarchical levels and a final image. In Fig. 9a, we can see that three groups of sub-regions are identified by using multiple core lines grown from seed points located within the long blue, small cyan, and tiny red sub-regions. Figure 9b shows that at a different threshold level, four groups of sub-regions are identified; note the additional tiny cyan blob. The

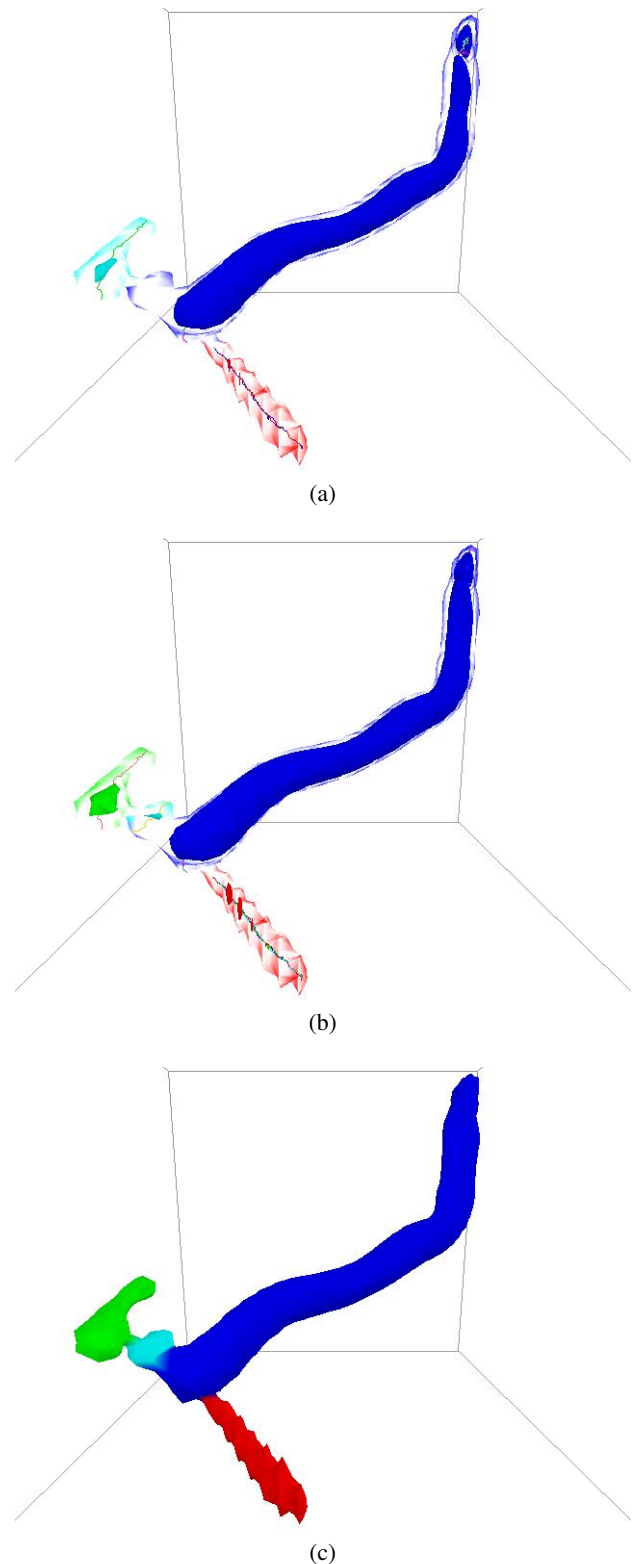


**Fig. 9** A success case of our algorithm. The top and middle images show the different segments that are identified at each intermediate level, and the bottom image shows the successful segmentation after multiple iterations.

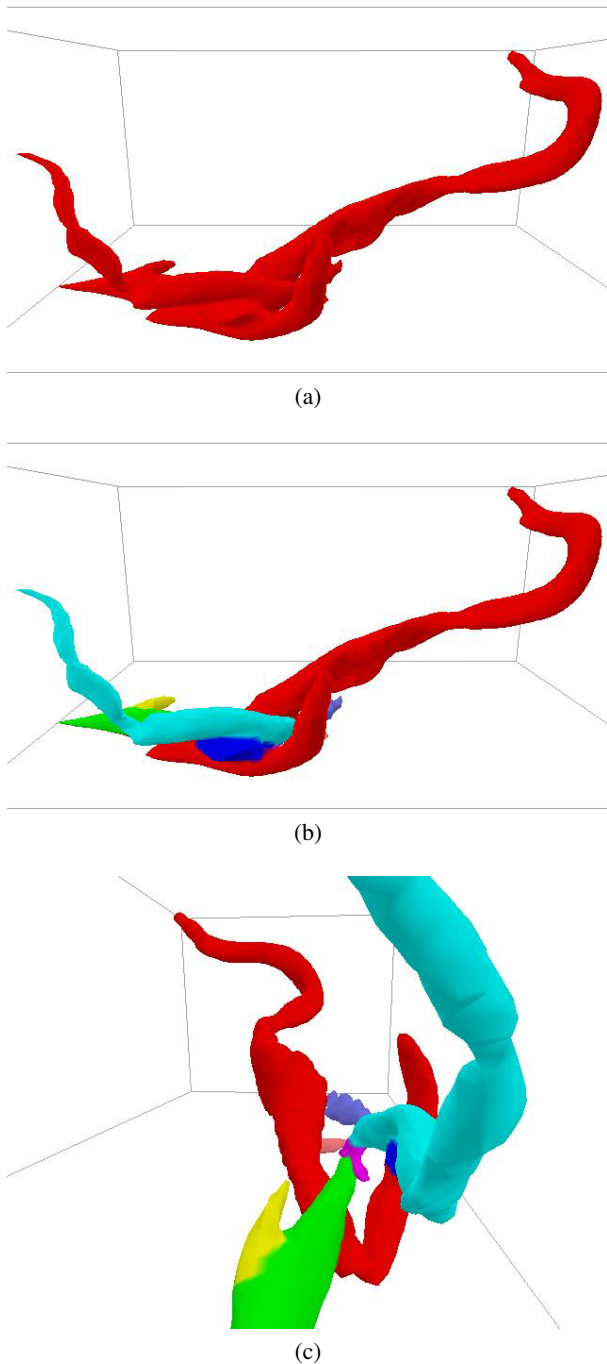


**Fig. 10** Another automatic segmentation produced by our algorithm. The top image shows one connected clump. The middle and bottom images show the segmentation result with eight individual vortices seen from different viewing angles.

green and cyan blobs in this figure were combined in the larger cyan region in Fig. 9a. The cyan structure in Fig. 9b is identified at the current swirl level but not at the previous levels. A transparent layer in these two images encompasses these candidate sub-regions and illustrates our interesting target clump. Different colors

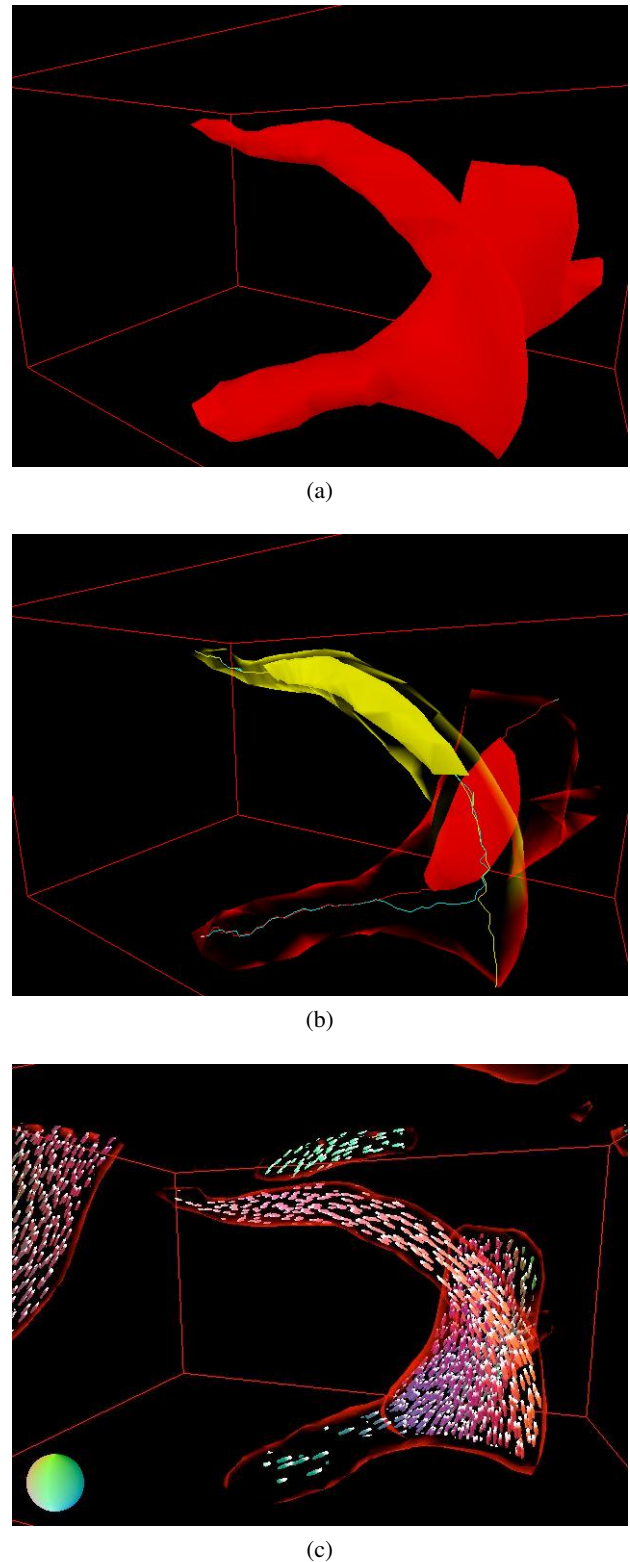


**Fig. 11** A failure case of our algorithm. Instability in the computation of the core lines leads to spurious divergences. This can be corrected for by locally comparing the vortex core line direction to the vorticity direction and terminating the core line following when the alignment becomes poor.

of a transparent layer represent different individual vortices corresponding to the candidate sub-regions at the current threshold level. Figure 9c shows the final result of our algorithm. Our approach considers all possible sub-regions detected at each threshold level to make an overall determination of the final segments that comprise a single coherent structure.

In Fig. 10, a compound structure identified in Fig. 7a has been automatically segmented into eight different subregions. Each of the component structures appears to be appropriately defined, with the possible exception of the large red structure which may or may not remain in a compound form. Figure 11 illustrates a failure case of our algorithm that requires some further effort to resolve. In Fig. 11b, we can see three core lines, colored red, yellow, and cyan, that were grown from seed points located within the large red and yellow subregions and within a tiny cyan sub-region barely visible near the upper end of the yellow colored segment. In this view, the yellow core line suggests a vortex that extends from the upper left to the lower right of the structure, and the red core line indicates a vortex that extends from the rear of the structure to the forward tip at the lower left corner of the image. The cyan core line begins by closely following the approximate path taken by the yellow core line, but then diverges (presumably as a result of numerical error) and eventually joins up with the red core line. Although this divergence is difficult to detect at a local level as it occurs, due to the universally noisy nature of the core line, we believe that there is good potential to flag such occurrences during a post process by double checking the correspondence between the direction indicated by the core line at any point and the directions indicated by the vorticity vectors at the surrounding points. If these directions are wildly discordant, we can not have confidence in the robustness of the path followed by the core line, and it should probably be truncated.

## 4 Conclusions

In this paper, we have presented two algorithms that can be used to identify individual vortex structures in volumetrically-defined 3-D turbulent flow datasets. These methods can be of use both to researchers who seek to quantify information about a flow at the level of individual structures, and also to those who want to be able to automatically track the evolution and interaction of large numbers

of individual vortices in a complicated turbulent flow. Our first method derives the underlying theoretical relationships among different measures of rotation direction in the flows. The possibility of using these properties for distinguishing different structures of vortices inspires new directions for research. The combined use of these multiple measures enables the superior segmentation of vortical structure compared with when only a single measure is used. Further investigation of proper selection of thresholds and advanced coherence of these measures with respect to the fluid dynamics are left for future work. Our second method is capable of successfully performing automatic segmentation on complex regions comprised of closely intertwined individual vortices that can not be distinguished by conventional types of vortex identification methods. However, our method may sometimes fail, particularly in situations where a continuous vortex core line can not be detected in the discrete data. The practical applications of our methods to time-varying datasets will be addressed in future work.

## Acknowledgements

This work was funded by the US National Science Foundation (No. CBET-0324898).

## Appendix

We begin by stating some well-known facts from linear algebra. Thinking of a vector  $\bar{v}$  as a  $3 \times 1$  matrix and its transpose  $\bar{v}^T$  as a  $1 \times 3$  matrix, the following can easily be proved:

### Lemma 1

- A.  $\bar{v}^T \bar{v} = |\bar{v}|^2$ .
- B.  $\bar{v}^T \bar{w} = \bar{w}^T \bar{v} = \bar{v} \circ \bar{w}$ .
- C.  $\bar{u} \circ (\bar{v} \times \bar{w}) = \bar{v} \circ (\bar{w} \times \bar{u}) = \bar{w} \circ (\bar{u} \times \bar{v})$ .
- D.  $\bar{v} \circ (\bar{w} \times \bar{v}) = 0$ .

More interesting is the following result.

Suppose the matrix  $A = \nabla V$  has one real eigenvalue  $\lambda$  with real eigenvector  $\bar{r}$  and a pair of complex conjugate eigenvalues and  $\lambda_1 = a + bi$  and  $\lambda_2 = a - bi$  with  $b > 0$ , with associated complex eigenvectors  $\bar{v}_1 = \bar{s} + \bar{t}i$  and  $\bar{v}_2 = \bar{s} - \bar{t}i$ . We can assume the eigenvectors are of unit length so  $1 = |\bar{v}_1|^2 = |\bar{s}|^2 + |\bar{t}|^2$ . Then, we can derive

$$A\bar{s} = \frac{A\bar{v}_1 + A\bar{v}_2}{2} = \frac{(a + bi)(\bar{s} + \bar{t}i) + (a - bi)(\bar{s} - \bar{t}i)}{2} = a\bar{s} - b\bar{t} \quad (1)$$

Similarly, we can show

$$A\bar{t} = b\bar{s} + a\bar{t}. \tag{2}$$

**Lemma 2** Let  $\bar{s} = \begin{pmatrix} s_1 \\ s_2 \\ s_3 \end{pmatrix}$ ,  $\bar{t} = \begin{pmatrix} t_1 \\ t_2 \\ t_3 \end{pmatrix}$ , and  $\bar{y} = \begin{pmatrix} u \\ v \\ w \end{pmatrix}$ . Then

$$\bar{t}^T \begin{pmatrix} 0 & w & -v \\ -w & 0 & u \\ v & -u & 0 \end{pmatrix} \bar{s} = \bar{y} \circ (\bar{t} \times \bar{s}).$$

**Proof**

$$\bar{t}^T \begin{pmatrix} 0 & w & -v \\ -w & 0 & u \\ v & -u & 0 \end{pmatrix} \bar{s} =$$

$$t_3(-s_2u + s_1v) + t_2(s_3u - s_1w) + t_1(-s_3v + s_2w) = u(s_3t_2 - s_2t_3) - v(s_3t_1 + s_1t_3) + w(s_2t_1 - s_1t_2) = \bar{y} \circ (\bar{t} \times \bar{s}). \blacksquare$$

We apply these results using Eqs. (1) and (2). Multiplying both side of Eq. (1) by  $\bar{t}^T$  and both side of Eq. (2) by  $\bar{s}^T$  we obtain

$$\begin{aligned} \bar{t}^T A\bar{s} &= a\bar{t}^T\bar{s} - b\bar{t}^T\bar{t}, \\ \bar{s}^T A\bar{t} &= b\bar{s}^T\bar{s} + a\bar{s}^T\bar{t}. \end{aligned}$$

Subtracting the first equation from the second we obtain

$$\bar{s}^T A\bar{t} - \bar{t}^T A\bar{s} = b(|\bar{s}|^2 + |\bar{t}|^2) \tag{3}$$

Using Lemma 1B, we rewrite  $\bar{s}^T A\bar{t}$  as  $\bar{t}^T A^T\bar{s}$ . Hence the left side of Eq. (3) becomes

$$\bar{t}^T (A^T - A)\bar{s} = \bar{t} \begin{pmatrix} 0 & Q_x - P_y & R_x - P_z \\ P_y - Q_x & 0 & R_y - Q_z \\ P_z - R_x & Q_z - R_y & 0 \end{pmatrix} \bar{s}.$$

But this is precisely the left hand side of the equation in Lemma 2 with  $\bar{y} = \bar{c}$ . We summarize this as Theorem 1.

**Theorem 1** Suppose  $\lambda_1 = a + bi$  and  $\lambda_2 = a - bi$  with  $b > 0$  are the complex eigenvalues and  $\bar{v}_1 = \bar{s} + \bar{t}i$  and  $\bar{v}_2 = \bar{s} - \bar{t}i$  with  $|\bar{s}|^2 + |\bar{t}|^2 = 1$  are the associated eigenvectors of the Jacobian  $\nabla V$  of a velocity vector field  $V$ . Then  $\bar{c} \circ \bar{n} = \bar{c} \circ (\bar{t} \times \bar{s}) = b(|\bar{s}|^2 + |\bar{t}|^2) = b$ , so that the angle  $\theta$  between  $\bar{c}$  and  $\bar{n}$  is given by

$$\cos \theta = \frac{b}{|\bar{c}| |\bar{t} \times \bar{s}|}.$$

Finding the angle between  $\bar{c}$  and  $\bar{r}$  is a bit more complicated. First we note that  $A\bar{r} = \lambda\bar{r}$  implies:

$$\begin{aligned} \bar{s}^T A\bar{r} &= \lambda(\bar{s}^T\bar{r}), \\ \bar{t}^T A\bar{r} &= \lambda(\bar{t}^T\bar{r}) \end{aligned} \tag{4}$$

Also from Eqs. (1) and (2) we can write

$$\begin{aligned} \bar{s}^T A^T\bar{r} &= \bar{r}^T A\bar{s} = a\bar{r}^T\bar{s} - b\bar{r}^T\bar{t}, \\ \bar{t}^T A^T\bar{r} &= \bar{r}^T A\bar{t} = b\bar{r}^T\bar{s} + a\bar{r}^T\bar{t} \end{aligned} \tag{5}$$

Subtracting Eqs. (4) from Eqs. (5) we get

$$\begin{aligned} \bar{s}^T (A^T - A)\bar{r} &= (a - \lambda)\bar{s}^T\bar{r} - b\bar{t}^T\bar{r}, \\ \bar{t}^T (A^T - A)\bar{r} &= b\bar{s}^T\bar{r} + (a - \lambda)\bar{t}^T\bar{r}. \end{aligned}$$

Using Theorem 1 together with Lemma 1C and Lemma 1D we obtain

$$\begin{aligned} \bar{s} \circ (\bar{r} \times \bar{c}) &= (a - \lambda)\bar{s}^T\bar{r} - b\bar{t}^T\bar{r}, \\ \bar{t} \circ (\bar{r} \times \bar{c}) &= b\bar{s}^T\bar{r} + (a - \lambda)\bar{t}^T\bar{r}, \\ \bar{r} \circ (\bar{r} \times \bar{c}) &= 0 \end{aligned} \tag{6}$$

If we let

$$\begin{aligned} B &= \begin{pmatrix} s_1 & s_2 & s_3 \\ t_1 & t_2 & t_3 \\ r_1 & r_2 & r_3 \end{pmatrix}, \\ \bar{x} &= \bar{r} \times \bar{c}, \\ \bar{w} &= \begin{pmatrix} (a - \lambda)\bar{s}^T\bar{r} - b\bar{t}^T\bar{r} \\ b\bar{s}^T\bar{r} + (a - \lambda)\bar{t}^T\bar{r} \\ 0 \end{pmatrix} \end{aligned} \tag{7}$$

we can rewrite Eqs. (6) as

$$B\bar{x} = \bar{w}.$$

Hence  $\bar{r} \times \bar{c} = B^{-1}\bar{w}$ . Then the angle  $\theta$  between  $\bar{r}$  and  $\bar{c}$  can be found using  $|\bar{r} \times \bar{c}| = |\bar{r}||\bar{c}| \sin \theta$ . We summarize this as Theorem 2.

**Theorem 2** If  $B$  and  $\bar{w}$  are as defined in Eqs. (7) then

$$\bar{r} \times \bar{c} = B^{-1}\bar{w}.$$

We can now prove Theorem 3 which we separate into three parts.

**Theorem 3.1** If  $\bar{r}$  and  $\bar{n}$  have the same direction, then  $\bar{c}$  is also in this direction.

**Proof** Suppose  $\bar{r}$  and  $\bar{n}$  have the same direction. Then  $\bar{r}$  is in the same direction as  $\bar{n} = \bar{t} \times \bar{s}$  and hence  $\bar{r}$  is perpendicular to both  $\bar{s}$  and  $\bar{t}$ . Then  $\bar{w}$  in Theorem 3 is the 0 vector and so  $\bar{r} \times \bar{c} = \bar{0}$ . But  $\bar{r} \times \bar{c} = \bar{0}$  only if  $\bar{r}$  and  $\bar{c}$  are in the same direction.  $\blacksquare$

**Theorem 3.2** If  $\bar{r}$  and  $\bar{c}$  have the same direction,

then  $\bar{n}$  is also in this direction.

**Proof** If  $\bar{r}$  and  $\bar{c}$  have the same direction, then  $\bar{r} \times \bar{c} = \bar{0}$ , so by Theorem 3,  $B^{-1}\bar{w} = \bar{0}$ . Hence  $\bar{w} = B\bar{0} = \bar{0}$ . But using the definition of  $\bar{w}$  in Eqs. (7) we can then write

$$\begin{pmatrix} a - \lambda & -b \\ b & a - \lambda \end{pmatrix} \begin{pmatrix} \bar{s}^T \bar{r} \\ \bar{t}^T \bar{r} \end{pmatrix} = \begin{pmatrix} 0 \\ 0 \end{pmatrix}.$$

The determinant of this matrix is  $(a - \lambda)^2 + b^2 \neq 0$ , so it is invertible and hence both  $\bar{s}^T \bar{r} = 0$  and  $\bar{t}^T \bar{r} = 0$ . But this means that  $\bar{r}$  is perpendicular to both  $\bar{s}$  and  $\bar{t}$  and hence  $\bar{r}$  is in the same direction as  $\bar{n} = \bar{t} \times \bar{s}$ . ■

**Theorem 3.3** If  $\bar{c}$  and  $\bar{n}$  have the same direction, then  $\bar{r}$  is also in this direction.

**Proof** Suppose  $\bar{c}$  and  $\bar{n}$  have the same direction. Then  $\bar{c} = k\bar{n}$  for some scalar  $k$ , so by Theorem 1

$$b = \bar{c} \circ \bar{n} = k\bar{n} \circ \bar{n} \quad (8)$$

Replacing  $\bar{c}$  in Eqs. (6) by  $k\bar{n}$  and using Lemma 1 C we obtain

$$\begin{aligned} \bar{r} \circ (k\bar{n} \times \bar{s}) &= (a - \lambda)\bar{s}^T \bar{r} - b\bar{t}^T \bar{r}, \\ \bar{r} \circ (k\bar{n} \times \bar{t}) &= b\bar{s}^T \bar{r} + (a - \lambda)\bar{t}^T \bar{r} \end{aligned} \quad (9)$$

which can be rewritten as

$$\begin{aligned} 0 &= \bar{r} \circ (k\bar{n} \times \bar{s} - (a - \lambda)\bar{s} + b\bar{t}) = \bar{r} \circ \bar{w}_1, \\ 0 &= \bar{r} \circ (k\bar{n} \times \bar{t} - b\bar{s} - (a - \lambda)\bar{t}) = \bar{r} \circ \bar{w}_2 \end{aligned} \quad (10)$$

Now  $k\bar{n} \times \bar{s}$  lies in the plane of  $\bar{s}$  and  $\bar{t}$  since it is perpendicular to  $\bar{n}$  so  $\bar{w}_1$  also lies in this plane. Similarly,  $\bar{w}_2$  lies in the plane of  $\bar{s}$  and  $\bar{t}$ . If we can show that  $\bar{w}_1$  and  $\bar{w}_2$  are linearly independent, and note from Eqs. (10) that  $\bar{r}$  is perpendicular to both of them then  $\bar{r}$  must be in the same direction as  $\bar{n}$ , the normal to this plane.

In order to show linear independence of  $\bar{w}_1$  and  $\bar{w}_2$ , we first note that

$$\begin{aligned} \bar{w}_1 \circ \bar{s} &= -(a - \lambda)(\bar{s} \circ \bar{s}) + b(\bar{t} \circ \bar{s}), \\ \bar{w}_2 \circ \bar{t} &= -b(\bar{s} \circ \bar{t}) - (a - \lambda)(\bar{t} \circ \bar{t}) \end{aligned} \quad (11)$$

Also, since

$$\begin{aligned} (k\bar{n} \times \bar{s}) \circ \bar{t} &= -k\bar{n} \circ (\bar{t} \times \bar{s}) = -k\bar{n} \circ \bar{n} = -b, \\ (k\bar{n} \times \bar{t}) \circ \bar{s} &= k\bar{n} \circ (\bar{t} \times \bar{s}) = k\bar{n} \circ \bar{n} = b, \end{aligned}$$

we obtain

$$\begin{aligned} \bar{w}_1 \circ \bar{t} &= -b - (a - \lambda)(\bar{s} \circ \bar{t}) + b(\bar{t} \circ \bar{t}), \\ \bar{w}_2 \circ \bar{s} &= b - b(\bar{s} \circ \bar{s}) - (a - \lambda)(\bar{t} \circ \bar{s}) \end{aligned} \quad (12)$$

To show linear independence we must show that  $c_1\bar{w}_1 + c_2\bar{w}_2 = \bar{0}$  implies that  $c_1 = c_2 = 0$ . But  $c_1\bar{w}_1 + c_2\bar{w}_2 = \bar{0}$  together with Eqs. (11) and (12) imply that

$$0 = c_1(\bar{w}_1 \circ \bar{s}) + c_2(\bar{w}_2 \circ \bar{s}) =$$

$$\begin{aligned} c_1(-(a - \lambda)(\bar{s} \circ \bar{s}) + b(\bar{t} \circ \bar{s})) + c_2(b - b(\bar{s} \circ \bar{s}) - (a - \lambda)(\bar{t} \circ \bar{s})), \\ 0 = c_1(\bar{w}_1 \circ \bar{t}) + c_2(\bar{w}_2 \circ \bar{t}) = \\ c_1(-b - (a - \lambda)(\bar{s} \circ \bar{t}) + b(\bar{t} \circ \bar{t})) + c_2(-b(\bar{s} \circ \bar{t}) - (a - \lambda)(\bar{t} \circ \bar{t})) \end{aligned} \quad (13)$$

We can write Eqs. (13) as

$$M \begin{pmatrix} c_1 \\ c_2 \end{pmatrix} = \begin{pmatrix} 0 \\ 0 \end{pmatrix},$$

where

$$M = \begin{pmatrix} -(a - \lambda)(\bar{s} \circ \bar{s}) + b(\bar{t} \circ \bar{s}) & b - b(\bar{s} \circ \bar{s}) - (a - \lambda)(\bar{t} \circ \bar{s}) \\ -b - (a - \lambda)(\bar{s} \circ \bar{t}) + b(\bar{t} \circ \bar{t}) & -b(\bar{s} \circ \bar{t}) - (a - \lambda)(\bar{t} \circ \bar{t}) \end{pmatrix}.$$

The determinant of  $M$  can be written as

$$((\bar{s} \circ \bar{s})(\bar{t} \circ \bar{t}) - (\bar{s} \circ \bar{t})^2)((a - \lambda)^2 + b^2)$$

which is greater than  $(a - \lambda)^2 + b^2$  by the Cauchy-Schwarz inequality. Hence  $M$  is invertible so  $c_1 = c_2 = 0$ . This completes the proof. ■

## References

- [1] R. J. Adrian, C. D. Meinhart, and C. D. Tomkins, Vortex organization in the outer region of the turbulent boundary layer, *J. Fluid Mech.*, vol. 422, pp. 1-54, 2000.
- [2] Q. Gao, C. Ortiz-Duenas, and E. K. Longmire, Analysis of vortex populations in turbulent wall-bounded flows, *J. Fluid Mech.*, vol. 678, pp. 87-123, 2011.
- [3] W. Jiang, R. Machiraju, and D. Thompson, Detection and visualization of vortices, in *The Visualization Handbook*, C. Hansen and C. Johnson, Eds., Elsevier Academic Press, 2004, pp. 295-326.
- [4] J. C. del Alamo, J. Jimenez, P. Zandonade, and R. D. Moser, Scaling of the energy spectra of turbulent channels, *J. Fluid Mech.*, vol. 500, pp. 135-144, 2004.
- [5] J. C. R. Hunt, A. A. Wray, and P. Moin, Eddies, streams and convergence zones in turbulent flows, in *Proc. 1988 Summer Program of the Center for Turbulence Research*, 1998, pp. 193-208.
- [6] M. S. Chong, A. E. Perry, and B. J. Cantwell, A general classification of three-dimensional flow fields, *Physics of Fluids*, vol. 2, no. 5, pp. 765-777, 1990.
- [7] J. Jeong and F. Hussain, On the identification of a vortex, *J. Fluid Mech.*, vol. 285, pp. 69-94, 1995.
- [8] J. Zhou, R. J. Adrian, S. Balachandar, and T. M. Kendall, Mechanisms for generating coherent packets of hairpin vortices in channel flow, *J. Fluid Mech.*, vol. 387, pp. 353-396, 1999.
- [9] D. Bauer and R. Peikert, Vortex tracking in scale-space, in *Proc. Joint Eurographics-IEEE TCVG Symposium on Visualization*, Barcelona, Spain, 2002, pp. 233-240.
- [10] D. Kenwright and R. Haimes, Automatic vortex core detections, *Computer Graphics and Applications*, vol. 13, no. 6, pp. 70-74, 1998.

- [11] M. Roth and R. Peikert, A higher-order method for finding vortex core lines, in *Proc. IEEE Visualization '98*, 1998, pp. 143-150.
- [12] J. Sahner, T. Weinkauff, and H. C. Hege, Galilean invariant extraction and iconic representation of vortex core lines, in *Proc. Joint Eurographics/IEEE VGTC Symposium on Visualization (EuroVis '05)*, Leeds, UK, 2005, pp. 151-160.
- [13] J. Sahner, T. Weinkauff, N. Teuber, and H. C. Hege, Vortex and strain skeletons in Eulerian and Lagrangian frames, *IEEE Transactions on Visualization and Computer Graphics*, vol. 13, no. 5, pp. 980-990, 2007.
- [14] T. Weinkauff, J. Sahner, H. Theisel, and H. C. Hege, Cores of swirling particle motion in unsteady flows, *IEEE Transactions on Visualization and Computer Graphics*, vol. 13, no. 6, pp. 1759-1766, 2007.
- [15] D. C. Banks and B. A. Singer, A predictor-corrector technique for visualizing unsteady flow, *IEEE Transactions on Visualization and Computer Graphics*, vol. 1, no. 2, pp. 151-163, 1995.
- [16] S. Stegmaier, U. Rist, and T. Ertl, Opening the can of worms: An exploration tool for vortical flows, in *Proc. IEEE Visualization 2005*, 2005, pp. 463-470.
- [17] M. Jankun-Kelly, M. Jiang, D. Thompson, and R. Machiraju, Vortex visualization for practical engineering applications, *IEEE Transactions on Visualization and Computer Graphics*, vol. 12, no. 5, pp. 957-964, 2006.
- [18] G. Haller, An objective definition of a vortex, *J. Fluid Mech.*, vol. 525, pp. 1-26, 2005.
- [19] F. Sadlo and R. Peikert, Efficient visualization of Lagrangian coherent structures by filtered AMR ridge extraction, *IEEE Transactions on Visualization and Computer Graphics*, vol. 13, no. 6, pp. 1456-1463, 2007.
- [20] R. Fuchs, R. Peikert, H. Hauser, F. Sadlo, and P. Muigg, Parallel vectors criteria for unsteady flow vortices, *IEEE Transactions on Visualization and Computer Graphics*, vol. 14, no. 3, pp. 615-626, 2008.
- [21] P. Chakraborty, S. Balachandar, and R. J. Adrian, On the relationships between local vortex identification schemes, *J. Fluid Mech.*, vol. 535, pp. 189-214, 2005.



**Shengwen Wang** received his PhD in the Department of Computer Science at the University of Minnesota in 2011, where his research focuses on scientific visualization, in particular, 3-D turbulent flow visualization and high dimensional data visualization. His recent interest also includes development of bioinformatics tools. He is currently an assistant researcher at the "National" Center for High Performance Computing in Taiwan, China.



**Jack Goldfeather** is the William H. Laird Professor of Mathematics, Computer Science, and the Liberal Arts in Carleton College, where he has been in the department since 1977. He received his MS (1971) and PhD (1975) degrees in mathematics at Purdue University. Over the years, he has done research in algebraic topology, chip design for rapid graphics display, tracking in virtual reality systems, and most recently in analyzing and visualizing vortex behavior in turbulent fluid flow.



**Ellen K. Longmire** joined the Department of Aerospace Engineering and Mechanics at the University of Minnesota in 1990. She received her MS (1985) and PhD (1991) degrees in mechanical engineering from Stanford University, where she specialized in experimental fluid mechanics. She uses experimentation and analysis to answer fundamental questions in fluid dynamics that affect industrial, biomedical, and environmental applications. Recently, her work has focused on single- and multi-phase turbulent flows, liquid/liquid mixtures with surface tension, microscale flows, and biomedical flows.



**Victoria Interrante** is an associate professor in the Department of Computer Science in the University of Minnesota. Her recent research focuses on the application of insights from perceptual psychology, art, and illustration to the design of more effective techniques for visualizing 3-D data. She received her PhD in computer science from the University of North Carolina at Chapel Hill in 1996.